Article

pubs.acs.org/Biomac

Synthesis, Characterization, and Antimicrobial Efficacy of Photomicrobicidal Cellulose Paper

Bradley L. Carpenter,[†] Frank Scholle,[‡] Hasan Sadeghifar,[§,∥] Aaron J. Francis,[†] Jonathan Boltersdorf,[†] Walter W. Weare,[†] Dimitris S. Argyropoulos,[†,§] Paul A. Maggard,[†] and Reza A. Ghiladi*[,†]

Departments of [†]Chemistry, [‡]Biological Sciences, and [§]Forest Biomaterials, North Carolina State University, Raleigh, North Carolina, 27695

[∥]Department of Wood and Paper Science, Sari Branch, Islamic Azad University, P.O. Box 48161-19318, Sari, Iran

Supporting Information

ABSTRACT: Toward our goal of scalable, antimicrobial materials based on photodynamic inactivation, paper sheets comprised of photosensitizer-conjugated cellulose fibers were prepared using porphyrin and BODIPY photosensitizers, and characterized by spectroscopic (infrared, UV−vis diffuse reflectance, inductively coupled plasma optical emission) and physical (gel permeation chromatography, elemental, and thermal gravimetric analyses) methods. Antibacterial efficacy was evaluated against *Staphylococcus aureus* (ATCC-2913), vancomycin-resistant *Enterococcus faecium* (ATCC-2320), *Acinetobacter baumannii* (ATCC-19606), *Pseudomonas aeruginosa* (ATCC-9027), and *Klebsiella pneumoniae* (ATCC-2146). Our best results were achieved with a cationic porphyrin−paper conjugate, **Por**$^{(+)}$-paper, with inactivation upon illumination (30 min, 65 ± 5 mW/cm^2, 400−700 nm) of all bacterial strains studied by 99.99+% (4 log units), regardless of taxonomic classification. **Por**$^{(+)}$-paper also inactivated dengue-1 virus (>99.995%), influenza A (∼99.5%), and human adenovirus-5 (∼99%). These results demonstrate the potential of cellulose materials to serve as scalable scaffolds for anti-infective or self-sterilizing materials against both bacteria and viruses when employing a photodynamic inactivation mode of action.

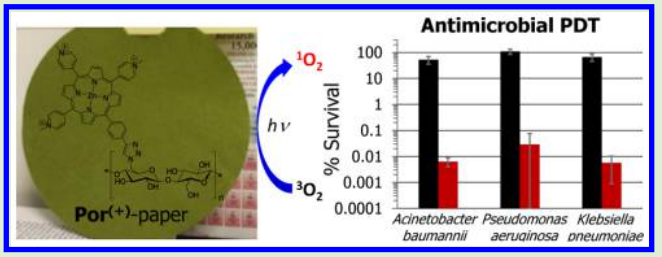

INTRODUCTION

As microbial drug resistance has increased in prevalence, previously treatable infections have re-emerged as serious and life-threatening healthcare challenges. Though typically not a direct threat to healthy individuals, drug-resistant nosocomial infections affect upward of 1 out of every 20 hospital patients in the United States,[1] contributing to the 100000 deaths attributed to hospital-acquired infections (HAIs) annually.[2] While many strategies to combat HAIs have been proposed, including new drug-discovery efforts, alternative treatment modalities, conservative use of antibiotics, and improvements to the FDA approval process,[3,4] preventative measures remain a crucial strategy in reducing the number of deaths due to HAIs. In light of this, a renewed focus on the development of advanced sterilization technologies and, in particular, self-sterilizing materials, has emerged as one such preventative strategy, since it has been found that strains of the most common bacterial pathogens can survive on hospital environment surfaces (e.g., bed linens, drapes, and counters) for prolonged periods of time prior to transmission.[5−10] Materials that are inherently antimicrobial could prevent the transmission of pathogenic microorganisms autonomously, without the potential for human error, leading to infections. These materials have the potential to contribute to a self-sterilizing hospital environment in a number of applications, including antimicrobial bedding, hospital drapes, patient gowns, staff uniforms, and countertops.[11,12] Such applications, however, currently remain only "potential" as our understanding of these materials, including their physical properties, scalability, scope of utilization, and efficacy as anti-infectives, is still developing.

There has been an increased interest in employing antimicrobial photodynamic inactivation (aPDI) as the basis for pathogen eradication given its advantages over other sterilization options.[13−16] These include (i) the photosensitizers, visible light, and material scaffolds themselves are nontoxic and are, therefore, not expected to have an adverse effect on human health; (ii) their antimicrobial action is primarily mediated by singlet oxygen,[17,18] which has several benefits including a short lifetime before it decays back to environmentally benign ground state (triplet) oxygen,[19] the ability to inactivate bacteria that are not in direct contact with the material,[20,21] as well as potentially broad antimicrobial efficacy against bacteria,[22−25] yeast,[26−29] viruses,[30−33] and parasites;[34,35] and (iii) as singlet oxygen causes nonspecific damage, it is thought that microbes will be unable to develop resistance to this mode of action.[24,36,37] Early investigations into aPDI materials were initially curtailed by the belief that, to be effective, photosensitizers needed to either be embedded in

Received: June 5, 2015
Revised: July 14, 2015
Published: July 16, 2015

DOI: 10.1021/acs.biomac.5b00758
Biomacromolecules 2015, 16, 2482−2492

the cellular envelope or internalized into the bacteria. This has been refuted as our scientific understanding of the mechanisms of antimicrobial photodynamic inactivation of bacteria has advanced, and consequently, a number of synthetic strategies for the conjugation of different classes of photosensitizers to synthetic and biopolymer-based scaffolds have been reported, including the use of esterification reactions,[38,39] the Cu(I)-catalyzed Huisgen-Meldal-Sharpless 1,3-dipolar cycloaddition reaction,[40−42] amine- or amide-linker forming conjugations,[43−45] as well as several other strategies.[46−48]

Toward our goal of scalable, self-sterilizing materials based on aPDI, we present here the preparation, characterization, and antimicrobial activity of paper sheets comprised of photosensitizer-conjugated cellulose fibers. Cellulose materials have many desirable physical characteristics,[49] including inherent biocompatibility, and provide an inexpensive and renewable starting material that is easily scalable. Our early work employing cellulose nanocrystals modified with a cationic porphyrin, termed CNC-Por,[41,42] validated this approach given the excellent antibacterial efficacy observed for that material. However, given the limitations of cellulose nanocrystals (e.g., limited scalability, additional preparation requirements),[50] we have instead chosen to work here with cellulose fibers. The corresponding antimicrobial paper sheets were prepared with a diverse set of photosensitizers, including cationic, anionic, and neutral porphyrins as well as neutral boron dipyrromethene (a.k.a. BODIPY, formally 4,4-difluoro-4-bora-3a,4a-diaza-s-indacene) based photosensitizers (Chart 1) and characterized

Chart 1. Antimicrobial Photosensitizer-Paper Sheets

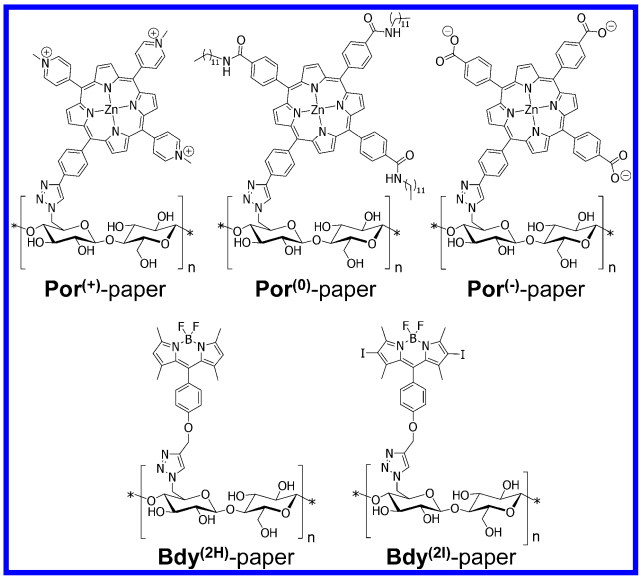

by spectroscopic (infrared, UV−vis diffuse reflectance, inductively coupled plasma optical emission) and physical (gel permeation chromatography, elemental and thermal gravimetric analyses) methods. The photosensitizer-conjugated paper sheets (PS-paper) were subsequently evaluated for their antibacterial efficacy against a set of taxonomically diverse bacteria, all of which were members of the so-called "ESKAPE" pathogens, known to be the most common causes of HAIs.[51] We also studied our most effective PS-paper against both enveloped and nonenveloped viruses to determine its antiviral efficacy. Our results demonstrate the potential for aPDI materials based on cellulose scaffolds to function effectively as anti-infective materials against both bacteria and viruses.

EXPERIMENTAL SECTION

Materials. Salts for the preparation of phosphate buffered saline solution were purchased from Fisher Scientific. Nutrient broth #234000 and heart brain broth #237500 were purchased from BD Difco, Miller LB broth was purchased from EMD Chemicals, and tryptic soy broth was purchased from Teknova. Whatman grade 1 filter paper was used to harvest cellulose fibers. UV−visible spectra were recorded on a Varian Cary 50 Bio spectrophotometer, and a Genesys 10 UV scanning spectrophotometer (Thermo Electron Corp.) was used for single wavelength measurements. A PerkinElmer 2400 CHNS analyzer was used for CHN elemental analysis. FTIR (Fourier transform infrared) spectra of photosensitizer-fiber conjugates were acquired on a Thermo Nicolet NEXUS 670 FT-IR spectrophotometer as KBr pellets. PS-fiber conjugate spectra in the range of 4000−650 cm^{-1} were obtained with a resolution of 4 cm^{-1} by accumulating 64 scans. UV−vis diffuse reflectance (UV−vis DRS) spectra were collected on a Shimadzu UV-3600 spectrophotometer equipped with an integrating sphere utilizing the wavelength range of 200−1500 nm. Thermal gravimetric analysis (TGA) was carried out on a TA Instruments TGAQ500 ramping 10 °C/min under N_2 purging.

Cellulose Fiber Preparation. Mother fibers were prepared from Whatman #1 filter paper. The filter paper was soaked with water for 2 h to open the fibers and then blended using a lab scale blender. After removing excess water, the fibers were washed 3× with acetone to clean and remove impurities. The fibers were subsequently dried at room temperature for 72 h and fluffed using a coffee grinder. Azido fibers and photosensitizer conjugated fibers were prepared (Scheme 1) with the same methodology as reported previously[41,42,52] using the cellulose fibers obtained here in lieu of the cellulose nanocrystals used in that earlier work.

Paper sheets were prepared from these fibers using the Tappi T205 sp-02 standard method.[53] The appropriate fibers were suspended in water to create a 1% (w/v) fiber suspension (1 g fibers/100 mL H_2O). The fibers were disintegrated using a TMI Durant Pulp Disintegrator at 3000 rpm for 10 min. The suspension was then transferred to a cylindrical British sheet making machine (173 mm diameter) and three additional liters of water were added. The water was then drained leaving a wet sheet that was further dried by pressing with blotting paper before bringing to dryness on a hot plate.

Porphyrin Loading onto Paper Sheets. The extent of porphyrin loading onto the fibers was determined using inductively coupled plasma-optical emission spectroscopy (ICP-OES). Samples were prepared by placing 1 custom hole punch of each paper sample (∼1 cm diameter) of known mass (listed in Table 2) into a 10 mL volumetric flask and bringing the volume to 10 mL by addition of 1 M HCl. The mixture was stirred vigorously at 60 °C for 2 h and then filtered prior to Zn analysis on a PerkinElmer Model 8000 Dual View ICP-OES spectrometer.

Gel Permeation Chromatography. GPC analysis was carried out with a Waters model ALC/GPC 204 (Waters Associates, Milford, MA) and 510 pump equipped with a UV detector (254 nm). The analysis was conducted at 40 °C using THF as the eluent at a flow rate of 0.7 mL/min. 200 μL of a 1 mg/mL solution of the analyte in THF was injected onto two Ultrastyragel columns (Styragel HR 1 and Styragel HR 5E, Waters) connected in series for analysis. Standard monodisperse polystyrenes (molecular weight ranges from 0.82 to 1860 kg/mol) were used for calibration. The number- (M_n) and weight- (M_w) average molecular weights were calculated using the Millenium 32 software.

Cell Culturing. All bacterial strains were grown in 5 mL cultures that were incubated on an orbital shaker at 37 °C. The growth conditions were as follows: *Acinetobacter baumannii* (ATCC-19606) was grown in Miller-LB media without antibiotics; methicillin-susceptible *Staphylococcus aureus* (ATCC-2913) was grown in tryptic soy broth media without antibiotics; *Pseudomonas aeruginosa* (ATCC-9027) was grown in BD Difco nutrient broth #234000; and *Klebsiella*

DOI: 10.1021/acs.biomac.5b00758
Biomacromolecules 2015, 16, 2482−2492

Scheme 1. General Route for the Synthesis of PS-Paper Conjugates

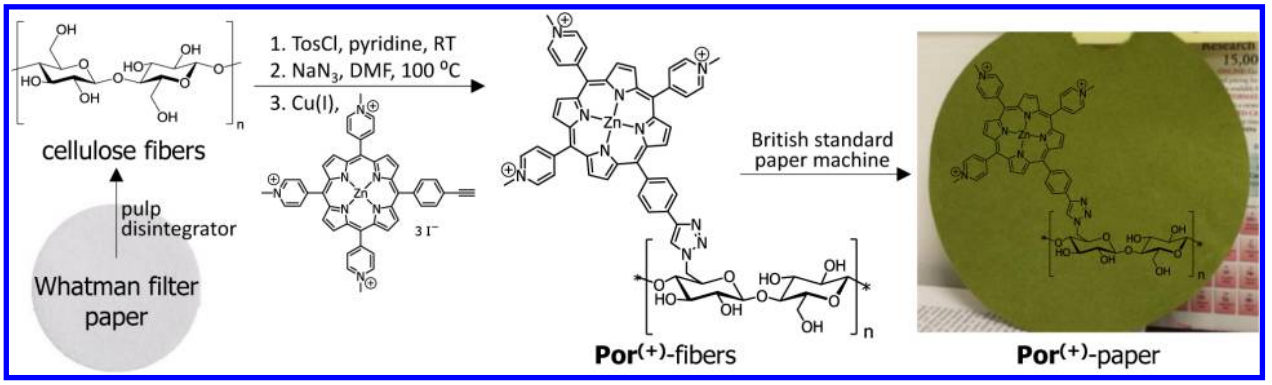

pneumoniae (ATCC-2146) was grown in BD Difco nutrient broth #234000 with 100 μg/mL ampicillin. The vancomycin-resistant strain of *Enterococcus faecium* (ATCC-2320) was grown in BD Difco Bacto brain heart infusion #237500 with 50 μg/mL ampicillin. Bacteria were grown to a concentration of 1−4 × 10^8 CFU/mL (determined spectrophotometrically from growth curves using a Genesys 10 UV scanning spectrophotometer) prior to being pelleted by centrifugation (10 min, ∼3700 g). Once pelleted, the supernatant was decanted, and the cells were resuspended in 5 mL of PBS (170 mM NaCl, 3.4 mM KCl, 10.0 mM Na_2HPO_4, 1.8 mM KH_2PO_4, pH 7.2).

Viral Propagation. The Dengue 1 virus was propagated for 168 h on C6/36 mosquito cells in L15 medium supplemented with 10% FBS (fetal bovine serum), antibiotics, and 10% tryptose phosphate broth before the virus was harvested. Human adenovirus-5 (HAd-5) was propagated for 96 h on the human lung carcinoma cell line A549 in DMEM (Dulbecco's Modified Eagle's Medium) with 10% FBS and antibiotics before the virus was harvested. Influenza A (PR8/34) was propagated for 48 h on Madine-Darby canine kidney cells (MDCK) in DMEM with 0.2% BSA (bovine serum albumin), 25 mM HEPES buffer (4-(2-hydroxyethyl)-1-piperazineethanesulfonic acid), antibiotics, and 2 μg/mL TPCK (tosyl phenylalanyl chloromethyl ketone)-treated trypsin before the virus was harvested. Antibiotics for all viral media were brought to a final concentration of 100 IU/mL penicillin, 100 IU/mL streptomycin, and 0.25 μg/mL fungizone.

Antimicrobial Photodynamic Inactivation Assay (aPDI). All photosensitization experiments were performed using a noncoherent light source, PDT light model LC122 (LumaCare, U.S.A.), equipped with a LUM V fiber optic probe (400−700 nm band-pass filter, average transmittance T_{avg} ∼95 ± 3%) and an OSRAM Xenophot halogen lamp model 93653 ELC-3/X (24 V, 250 W). The fluence rate was measured with an Orion power meter (Orphir Optronics Ltd., Israel). All experiments were carried out in triplicate at a minimum (unless noted otherwise), and statistical significance was assessed via a two-tailed, unpaired Student's *t* test.

Bacteria. For each antibacterial PDI trial, duplicate 24-well plates (Nunc, flat bottom) were prepared by placing into adjacent wells one circular sheet of Whatman grade 1 filter paper (as a PS-free control) and one circular sheet of PS-modified paper. Each sheet was cut to precisely fit the well bottom (∼1 cm diam.) using a custom hole-punch. A 100 μL aliquot of a single 5 mL bacterial culture was then added to each of the four wells. Once inoculated, one of the well plates was kept in the absence of light as a dark control, and the other was illuminated for 30 min at 65 ± 5 mW/cm^2 with noncoherent visible light (400−700 nm). Following illumination, 1 mL of sterile PBS was added to each well in both the illuminated and the dark control plate, and the bacteria were resuspended with vigorous stirring and vortexing. Each well was 1:10 serially diluted (40 μL into 360 μL aliquots of PBS) five times, and 10 μL from the undiluted and each diluted well were plated in columns on gridded six column square agar plates made with their respective growth media (without antibiotics). The plates were incubated overnight in the dark at 37 °C. The survival rate was determined by the ratio of CFU/mL of the illuminated sample versus that of the identical paper from the dark control. The minimum detection limit was 100 CFU/well (based on the plated 10 μL aliquot from the 1 mL undiluted well). Variations in the number of delivered CFUs (1−4 × 10^7 CFUs from the broth culture at a concentration of 1−4 × 10^8 CFU/mL) resulted in a detection limit range of 0.01−0.001% survival.

Viruses. Antiviral photodynamic inactivation studies were carried out with a methodology similar to that of the antibacterial studies. Three sheets of both Whatman grade 1 filter paper (PS free control) and **Por**$^{(+)}$-paper were cut using a standard hole-punch (5 mm) to closely fit the well bottom of a 96-well plate (Olympus). Virus (25 μL) was added both to the wells with paper sheets and to three without (no paper control), and the plate was then illuminated for 30 min at 65 ± 5 mW/cm^2 with noncoherent visible light (400−700 nm). Another 96 well plate, prepared identically to the first, was kept in the absence of light as a dark control. Following illumination, 100 μL of MEM (Eagle's Modified Essential Medium) with 1% FBS, 10 mM HEPES, and 1% antibiotics were added to each well in both the illuminated and dark control plates. The wells were gently vortexed with a micropipettor to facilitate removal of the viruses from the paper sheets, and each well was 1:10 serially diluted (15 μL into 135 μL aliquots of MEM) six times. To gauge the viral concentration in each of the wells, the viruses were titered on the appropriate cell lines: the Vero E6 cell line was used for titering the dengue 1 virus, the A549 cell line for human adenovirus-5, and the MDCK cell line for the influenza A virus. Each of these target cell lines were grown to confluence in 24 well plates (Falcon, flat bottom). The confluent cells were then infected with 150 μL of the serial dilutions. After 1 h of incubation, 800 μL of a semisolid overlay (1% tragacanth gum in MEM) was added, and the plates were incubated for 24 h (influenza A/MDCK) or 72 h (human adenovirus-5/A549 and dengue-1/Vero E6). For the influenza A virus and MDCK cell line, 2 μg/mL of TPCK-treated trypsin was also added to the semisolid overlay prior to incubation. Each of the wells was fixed with 50:50 acetone/methanol, blocked with 1% normal horse serum for 10 min, and incubated with primary antibodies specific to the viruses: E-protein specific antibody D1−4G2 was used for the dengue 1 virus, adenovirus-2/5 E1A (A-3) antibody (Santa Cruz Biotechnology) for HAd-5, and an HA-specific antibody (C102; Thermo Scientific) for the influenza A virus. Immunofoci were visualized after incubation with horseradish peroxidase conjugated antimouse IgG and staining using the Vectastain ABC kit specific to mouse IgG (Vector Laboratories). Foci in wells containing 20−70 foci (depending on the virus) were counted for the calculation of focus-forming units (FFU). While the concentration detection limit was 50 FFU/mL for each virus, due to differences in starting viral concentration, the detection limit for % activity varied between viruses as follows: dengue-1 virus, 99.995%; influenza A, 99.5%; human adenovirus-5, 99.95%.

RESULTS

Synthesis. A general route for the covalent attachment of alkyne-bearing photosensitizers to azide-functionalized cellulose fibers (N_3-fibers) using the Cu(I)-catalyzed Huisgen-Meldal-

DOI: 10.1021/acs.biomac.5b00758
Biomacromolecules 2015, 16, 2482−2492

Sharpless 1,3-dipolar cycloaddition reaction is shown (Scheme 1). The structures of the alkyne-bearing photosensitizers $Por^{(+)}$ (**1**), $Por^{(0)}$ (**2**), $Por^{(-)}$ (**3**), $Bdy^{(2H)}$ (**4**), and $Bdy^{(2I)}$ (**5**) are provided in Chart S1 and their syntheses are described in the Supporting Information. Azide-functionalized cellulose fibers (N_3-fibers) and conditions for the azide/alkyne coupling reaction followed literature precedent[41,42] with minor modifications, notably that cellulose fibers were employed here in lieu of cellulose nanocrystals used previously.

Once pressed into paper sheets, **Por**$^{(+)}$-paper and **Por**$^{(-)}$-paper were prepared and used without further modification. However, for **Por**$^{(0)}$-paper, **Bdy**$^{(2H)}$-paper and **Bdy**$^{(2I)}$-paper, it was found that PBS and deionized water beaded on the paper surfaces due to their hydrophobicity. As the goal of this study was to evaluate the photomicrobiocidal properties of the papers rather than create a water-impermeable barrier, these photosensitizer modified fibers were mixed (doped) with either 25 wt % (for $Bdy^{(2H)}$ and $Bdy^{(2I)}$) or 50 wt % (for $Por^{(0)}$) unmodified cellulose mother fibers to increase the hydrophilicity of the resulting paper, thereby enabling the bacterial/viral cultures in PBS to absorb into the sheets for subsequent photosensitization studies. It was observed that the doping process increased the error for the associated aPDI studies of these papers (vide infra) that is likely due to the heterogeneity in photosensitizer distribution arising from the incomplete mixing of the PS-conjugated and mother fibers in the resulting paper.

Characterization. *FTIR Characterization of Photosensitizer Modified Fibers.* Prior to being pressed into paper sheets, FTIR spectroscopy was used to assess azide addition to the mother fibers (yielding N_3-fibers), as well as the conjugation of the photosensitizers (yielding PS-fibers). The FTIR spectra were normalized to the cellulose C−O stretching vibration at 1030 cm^{-1}.[54] The N_3-fiber spectra (Figure 1, panels A and B, black trace) show a clear azide band at 2113 cm^{-1}, confirming the presence of the azide-modified cellulose fibers. The amount of azide loading, as determined by the area of this band in the normalized spectra, was found to be lower in N_3-fibers than in the previously studied cellulose nanocrystals[41] and can be rationalized given the lower percent surface area of the fibers relative to the cellulose nanocrystals. Since the Huisgen-Meldal-Sharpless 1,3-dipolar cycloaddition reaction converts azide functional groups to triazole linkers, the addition of photosensitizers to the N_3-fibers correlates with a % reduction in the azide band area: the **Por**$^{(+)}$-fiber spectrum (Figure 1A, red trace) shows a decline in the azide band area (~30%), consistent with covalent attachment of the photosensitizer, albeit at a lower efficiency than that observed for this reaction when employing azide-functionalized cellulose nanocrystals (72%).[41] Interestingly, the spectrum of the **Por**$^{(-)}$-fibers (Figure 1A, green trace) showed a greater extent of photosensitizer conjugation than did **Por**$^{(+)}$-fibers, with the azide band significantly reduced (>90%) in intensity. This higher loading may be partly due to a lower electrostatic repulsion effect for **Por**$^{(-)}$ (**3**), as this porphyrin was conjugated to the N_3-fibers in its triprotic/neutral form, resulting in less charge−charge repulsion than in the **Por**$^{(+)}$-fiber reaction that utilized the cationic porphyrin in the corresponding conjugation reaction. The **Por**$^{(0)}$-fiber spectrum (Figure 1A, orange trace) also showed no azide peak. However, because FTIR analysis was carried out after doping with 50 wt % mother fibers, the lack of an azide band is attributable to the combination of the dilution with mother fibers (see elemental analysis and ICP-OES for further discussion, vide infra) as well as due to the photosensitizer conjugation. An additional feature seen in the spectrum of the **Por**$^{(0)}$-fiber is the reduction of the large absorbance at ~3300 cm^{-1}. This may also be a result of the doping process, or it could be due to the lower hygroscopic nature of the neutral **Por**$^{(0)}$-fiber, causing it to absorb less water from its environment.

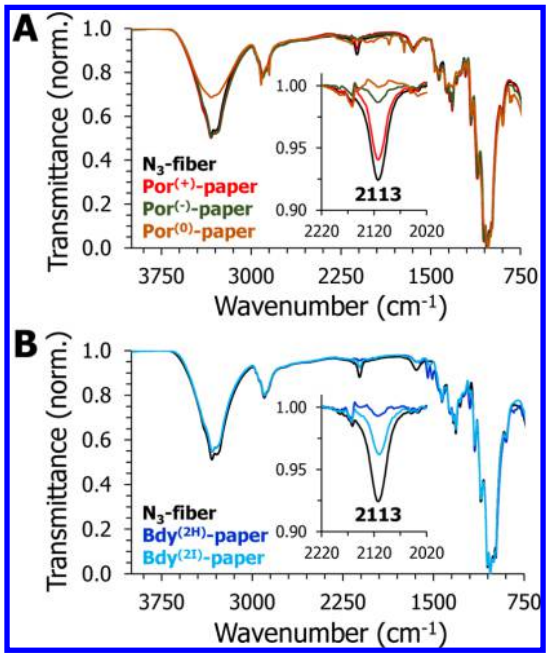

Figure 1. FTIR spectra of (A) N_3-fiber (black), **Por**$^{(+)}$-fiber (red), **Por**$^{(0)}$-fiber (orange), and **Por**$^{(-)}$-fiber (green), and (B) N_3-fiber (black), **Bdy**$^{(2H)}$ (blue), and **Bdy**$^{(2I)}$ (light blue).

The FTIR spectra of **Bdy**$^{(2H)}$-fibers (blue) and **Bdy**$^{(2I)}$-fibers (light blue) are shown in Figure 1B. Only a trace azide band can be observed in the **Bdy**$^{(2H)}$-fiber spectrum, suggesting near complete surface modification. By contrast, **Bdy**$^{(2I)}$-fiber showed lower reactivity in comparison to the dihydro analog, but still exhibited a ~50% reduction in the azide band when compared with the precursor N_3-fibers. Overall, both BODIPY compounds were observed to have greater reactivity with N_3-fibers than $Por^{(+)}$ (**1**), supporting the hypothesis that lower charge−charge repulsion leads to greater surface modification, although the smaller size of the BODIPY photosensitizers may be a factor as well. It should be noted that these spectra were recorded prior to the doping of **Bdy**$^{(2H)}$-fiber and **Bdy**$^{(2I)}$-fiber with mother fibers.

Gel Permeation Chromatography. The molecular weight gain attributable to the appended photosensitizers for **Por**$^{(+)}$-paper and **Bdy**$^{(2I)}$-paper was assessed by gel permeation chromatography (GPC). Due to the insolubility of cellulosic samples in organic solvents, the hydroxyl groups were benzoylated prior to GPC analysis: samples of **Por**$^{(+)}$-paper and **Bdy**$^{(2I)}$-paper were dissolved in the ionic liquid 1-allyl-3-methylimidazolium chloride [(Amin)$^+$Cl$^-$] and treated with benzoyl chloride. The weight-average molecular weight (M_w), number-average molecular weight (M_n), and consequently the distribution of molecular weight also known as polydispersity (M_w/M_n) were calculated from the GPC data. The weight-average molecular weight (M_w) distributions of **Por**$^{(+)}$-paper and **Bdy**$^{(2I)}$-paper were found to be 212000 g/mol and 217000 g/mol, respectively (Figure 2, Table 1). As these values represent a slight gain when compared to the precursor N_3-fiber

DOI: 10.1021/acs.biomac.5b00758
Biomacromolecules 2015, 16, 2482−2492

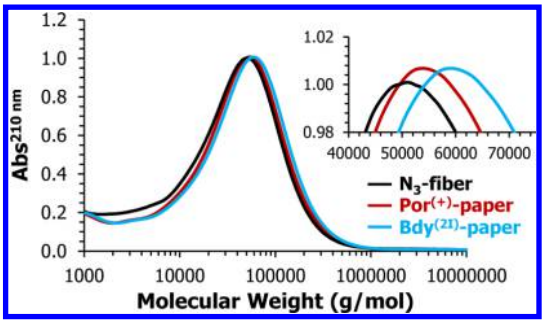

Figure 2. Gel permeation chromatographs of benzoylated derivatives of N_3-fiber (black), **Por**$^{(+)}$-paper (red), and **Bdy**$^{(2I)}$-paper (light blue) in THF.

Table 1. Molecular Weight Distributions of Benzoylated Derivatives of N_3-Fiber, Por$^{(+)}$-Paper, and Bdy$^{(2I)}$-Paper in THF

	weight-average molecular weight (M_w) 10^3 g/mol	number-average molecular weight (M_n) 10^3 g/mol	polydispersity (M_w/M_n)
N_3-fiber	202	55	3.67
Por$^{(+)}$-paper	212	57	3.72
Bdy$^{(2I)}$-paper	217	58	3.74

(202000 g/mol), and in light of the error in the measurement,[55] an exact determination regarding the photosensitizer loading was not possible. Rather, from the molecular weight increase and considering the average formula mass of the anhydrous glucose unit of 162 g/mol, the upper limit of photosensitizer loading was estimated as one photosensitizer molecule per 100 glucose molecules. No significant changes in polydispersity (M_w/M_n) were noted (Table 1).

Porphyrin Loading. Each free base porphyrin was metalated with zinc prior to the Cu(I)-catalyzed cycloaddition reaction to prevent undesired copper−metalation, as copper porphyrins exhibit extremely poor photophysical properties with respect to singlet oxygen generation.[56] ICP-OES was used to determine the Zn concentration in the porphyrin-paper materials, which is equivalent to the porphyrin loading if complete metalation of the porphyrin is assumed (as supported by UV−vis diffuse reflectance spectroscopy, vide infra). The **Por**$^{(-)}$-paper was found to have the highest porphyrin loading at 33.2 nmol porphyrin per mg of paper (Table 2), in agreement with the

Table 2. ICP-OES Zn Analysis of the Porphyrin-Modified Papers

material	sample mass (mg)	nmol porphyrin/sheet	nmol porphyrin/mg paper
Por$^{(+)}$-paper	13.1	168	12.4
Por$^{(0)}$-paper	28.5	101	3.54
Por$^{(-)}$-paper	17.2	570	33.2

FTIR results. The **Por**$^{(+)}$-paper was found to have a loading of 12.4 nmol porphyrin per mg paper. This calculates to approximately one-third the amount of porphyrin loading in comparison to **Por**$^{(-)}$-paper and again closely agrees with the FTIR data. The doped **Por**$^{(0)}$-paper was found to have a loading of 3.54 nmol porphyrin per mg paper, implying that the predoped fibers would have ∼7 nmol porphyrin per mg paper, still only about half that of the **Por**$^{(+)}$-paper and less than a fourth that of the **Por**$^{(-)}$-paper. This strongly suggests that

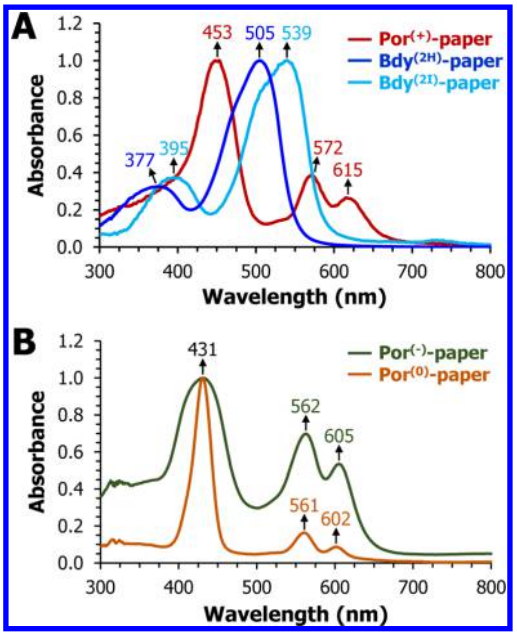

Figure 3. UV−vis diffuse reflectance spectroscopy of (A) **Por**$^{(+)}$-paper, red; **Bdy**$^{(2H)}$-paper, blue; **Bdy**$^{(2I)}$-paper, light blue; and (B) **Por**$^{(-)}$-paper, green; **Por**$^{(0)}$-paper, orange.

Por$^{(0)}$ (**2**) had a lower efficiency in its reaction with the N_3-fibers when compared to the other porphyrin-based photosensitizers. This lower loading could be attributable to the large size of the aliphatic groups leading to steric hindrance with the N_3-fibers. ICP-OES was not performed on **Bdy**$^{(2H)}$-paper or **Bdy**$^{(2I)}$-paper since neither photosensitizer possessed Zn (or another metal that could be comparably analyzed).

UV−Vis Diffuse Reflectance Spectroscopy. The UV−vis diffuse reflectance spectrum of **Por**$^{(+)}$-paper [453 (Soret), 572, 615 nm] (Figure 3) in the solid state was found to be shifted bathochromically from that of Por$^{(+)}$ (**1**) [UV−visible (H_2O): 436 (Soret), 564, 608 nm] in solution. Such bathochromic shifts have been previously[42] attributed to the differences in the local environment (e.g., polarity and solvation) of the porphyrin due to the presence of the covalently appended cellulose for **Por**$^{(+)}$-CNCs [UV−visible: 442 (Soret), 567, 612 nm for the benzoylated analog], and we suggest a similar solvation-dependence here. **Bdy**$^{(2I)}$-paper [395, 539 nm] showed only minor (<5 nm) shifts in absorbance from its precursor compound. **Por**$^{(-)}$-paper [431 (Soret), 562, 605 nm] and **Por**$^{(0)}$-paper [431 (Soret), 561, 602 nm] showed only minor shifts from the spectra of their precursor compounds Por$^{(0)}$ (**2**) and Por$^{(-)}$ (**3**). Overall, the results suggest that no significant changes to the porphyrin or BODIPY precursors, including no transmetalation with the copper catalyst or loss of metal yielding the free-base porphyrin, occurred during the Huisgen-Meldal-Sharpless 1,3-dipolar cycloaddition reaction (other than that of solvation). Metalation with copper would lead to significant changes in the absorption spectrum as noted previously.[57]

Thermal Gravimetric Analysis. Thermal gravimetric analysis was performed on the unmodified mother fibers, N_3-fibers, **Por**$^{(+)}$-paper, and **Bdy**$^{(2I)}$-paper to gain an understanding of the thermal stability of these materials (Figure 4). Apart from a minor initial weight loss that was observed for all materials up to 100 °C (attributable to loss of water), each was found to be stable in excess of 250 °C. The mother fibers (purple) proved

DOI: 10.1021/acs.biomac.5b00758
Biomacromolecules 2015, 16, 2482−2492

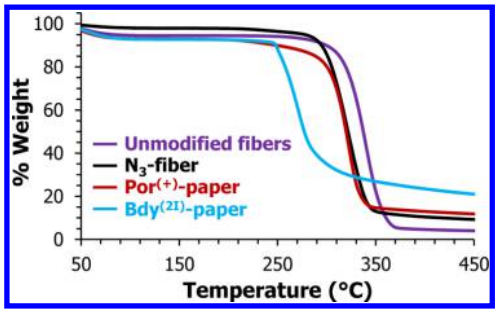

Figure 4. Thermal gravimetric analysis of mother fibers (purple), N_3-fiber (black), **Por**$^{(+)}$-paper (red), and **Bdy**$^{(2I)}$-paper (light blue).

the most robust to thermal degradation (up to ~330 °C), followed by N_3-fiber (black, ~290 °C), in line with previous measurements.[41] **Por**$^{(+)}$-paper (red) also exhibited excellent thermostability, with substantial mass reduction only observed above 290 °C. In comparison, cellulose nanocrystals modified with Por$^{(+)}$ (**1**), CNC-Por,[41] afforded a material with a similar thermal gravimetric behavior: minor degradation commencing around 210 °C (weight loss of <20%), with major decomposition above 320 °C. The **Bdy**$^{(2I)}$-paper (light blue) was found to be the least thermostable, with significant weight loss occurring at ~250 °C.

Antimicrobial Activity Results. *PDI Studies Employing Por*$^{(+)}$*-Paper.* In vitro aPDI studies employing the cationic porphyrin-based **Por**$^{(+)}$-paper were performed under fixed illumination conditions (30 min, 400−700 nm, 65 ± 5 mW/cm^2) to enable comparisons with previous studies that employed **Por**$^{(+)}$-CNCs.[41,42] The two Gram-positive bacteria, *S. aureus* ATCC-2913 and the vancomycin-resistant *E. faecium* (VRE) strain ATCC-2320, were found to be highly susceptible to photodynamic inactivation with **Por**$^{(+)}$-paper: upon illumination, *S. aureus* was inactivated greater than 99.997% (~5 log units, $P < 0.05$; Figure 5A), and vancomycin-resistant *E. faecium* (ATCC-2320) by 99.987% (~4 log units, $P < 0.005$; Figure 5A). By contrast, under the same illumination conditions the bacteria exhibited 100% survival on the unmodified cellulose paper (PS-free control), demonstrating the requirement of the photosensitizer for bacteria inactivation. The dark controls employing **Por**$^{(+)}$-paper did initially show some inactivation when the serial dilution step was performed under ambient room light exposure (data not shown), but this was eliminated by using low room lighting conditions (e.g., a darkroom red light that emitted at wavelengths where the photosensitizers did not absorb well), and the workup for both dark and light plates were ultimately performed under these conditions. In comparison with **Por**$^{(+)}$-paper, results employing the identical cationic photosensitizer conjugated to cellulose nanocrystals (**Por**$^{(+)}$-CNCs) demonstrated a comparable level of inactivation (~6 log units) under identical conditions for *S. aureus*,[41,42] and together they suggest that cellulose fibers are as effective a scaffold as cellulose nanocrystals despite their lower surface area.[41,42] While the *E. faecium* strain was not previously tested against **Por**$^{(+)}$-CNCs, this bacterium has also been shown to be highly susceptible to photodynamic inactivation in other studies.[58]

Gram-negative bacteria are typically more resistant to photodynamic inactivation than Gram-positive species due to their additional outer membrane with highly impermeable lipopolysaccharides.[59] Surprisingly, however, **Por**$^{(+)}$-paper showed virtually identical efficacy against Gram-negative

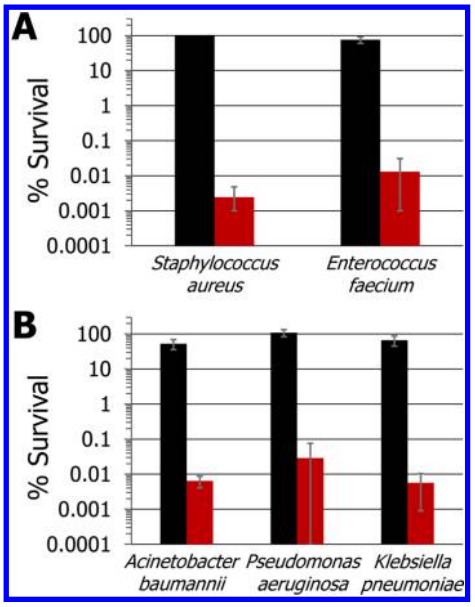

Figure 5. Photodynamic inactivation studies employing **Por**$^{(+)}$-paper. (A) Gram-positive species: methicillin-susceptible *S. aureus* (MSSA) ATCC-2913 and the vancomycin-resistant *E. faecium* (VRE) ATCC-2320 strain. (B) Gram-negative species: *A. baumannii* ATCC-19606, *P. aeruginosa* ATCC-9027, and *K. pneumoniae* ATCC-2146. The black bars represent the % survival of the illuminated PS-free control as a percent of the dark PS-free control, whereas the red bars represent the % survival of the illuminated **Por**$^{(+)}$-paper as a percent of the dark control of **Por**$^{(+)}$-paper. For all bacteria, the illumination conditions were as follows: 30 min, 400−700 nm, and 65 ± 5 mW/cm^2 (total fluence of 118 J/cm^2). As the plating technique employed to determine % survival did not allow for detection of survival rates of <0.0001%, data points below the detection limit were set to 0.0001% survival for graphing purposes. In the cases where error bars cannot be visualized, the error bars themselves were smaller than the marker employed in the plot.

bacteria (Figure 5B) when compared to the Gram-positive strains above. Specifically, *Acinetobacter baumannii* ATCC-19606 was photoinactivated by **Por**$^{(+)}$-paper to 99.997% reduction in CFU/mL (~5 log units; $P < 0.05$), *Pseudomonas aeruginosa* ATCC-9027 to 99.97% reduction (~4 log units; $P < 0.001$), and the multidrug resistant NDM-1-producing *K. pneumoniae* clinical isolate ATCC-2146 explored here was inactivated to 99.994+% reduction (4.5 log units; $P < 0.05$). Interestingly, while **Por**$^{(+)}$-CNCs achieved a similar level of photoinactivation against *A. baumannii*,[42] they were less effective (<2.5 log units inactivation) against *P. aeruginosa*, highlighting a difference between these two materials in favor of **Por**$^{(+)}$-paper.

Finally, the effects of extended photobleaching were examined by preilluminating the **Por**$^{(+)}$-paper sheet continuously for 12 h under the same illumination conditions as the aPDI studies (400−700 nm, 65 ± 5 mW/cm^2), followed by repetition of the *A. baumannii* trial employing this "photoaged" paper. No statistically significant loss in antimicrobial activity was noted when compared to the results in Figure 5B (data not shown), suggesting the material has excellent robustness over the time period examined. Overall, our results against both Gram-positive and Gram-negative bacteria are particularly noteworthy in the context of "ESKAPE" pathogens[51,60] given the broad photoinactivation efficacy of **Por**$^{(+)}$-paper against the bacterial strains examined here regardless of their drug-

DOI: 10.1021/acs.biomac.5b00758
Biomacromolecules 2015, 16, 2482−2492

resistance phenotype (ESKAPE = acronym for the most common nosocomial infectious agents, *Enterococci faecium*, *Staphylococcus aureus*, *Klebsiella pneumoniae*, *Acinetobacter baumannii*, *Pseudomonas aeruginosa*, and *Enterobacter* species).

PDI Studies Employing Bdy$^{(2H)}$-Paper and Bdy$^{(2I)}$-Paper. The boron-dipyrromethene-based **Bdy$^{(2H)}$**-paper and **Bdy$^{(2I)}$**-paper were also investigated for their aPDI efficacy. For **Bdy$^{(2H)}$**-paper, little to no significant inactivation of Gram-positive (Figure 6A) or Gram-negative (Figure 6B) bacteria was observed. This result was not unexpected, as the lack of heavy atoms on the BODIPY photosensitizer scaffold leads to a high fluorescence quantum yield that is an alternative relaxation pathway (nonproductive) to that of singlet oxygen generation.[23,61] Notably, this result serves to confirm that there is little to no nonphotodynamic antimicrobial activity associated with these materials. As expected, the **Bdy$^{(2I)}$**-paper results were generally better than **Bdy$^{(2H)}$**-paper, with the one notable exception that the vancomycin-resistant *E. faecium* (VRE) ATCC-2320 strain was not statistically different from the dark control. *S. aureus* ATCC-2913 was inactivated >90% (~1 log unit; $P < 0.01$). Interestingly, **Bdy$^{(2I)}$**-paper proved more effective against the Gram-negative bacteria when compared to the Gram-positive strains: both *A. baumannii* ATCC-19606 and *P. aeruginosa* ATCC-9027 were inactivated with similar efficiency to 99.5% reduction in CFU/mL (2.5 log units), though with limited statistical significance, as the latter was performed only in duplicate. *K. pneumoniae* ATCC-2146 was inactivated slightly less than the other two strains to ~90% reduction in CFU/mL (1 log unit; $P < 0.01$). This may indicate a greater sensitivity of Gram-negative species than their Gram-positive counterparts to the neutral BODIPY-based photosensitizer, but this was not further explored, as the overall efficacy of **Bdy$^{(2H)}$**-paper and **Bdy$^{(2I)}$**-paper was substantially poorer than **Por$^{(+)}$**-paper for all bacteria examined here.

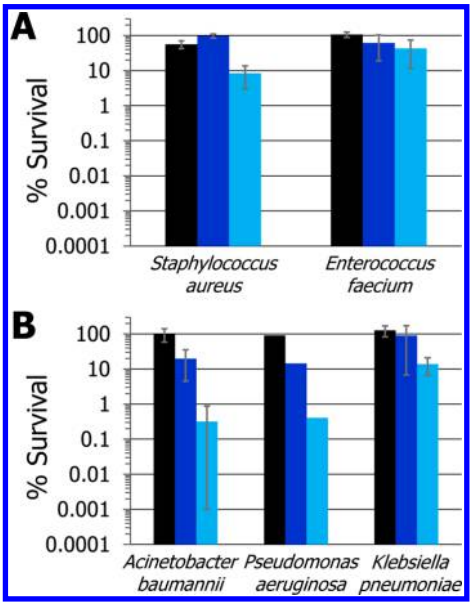

Figure 6. Photodynamic inactivation studies employing **Bdy$^{(2H)}$**-paper and **Bdy$^{(2I)}$**-paper. (A) Gram-positive species: methicillin-susceptible *S. aureus* (MSSA) ATCC-2913 and the vancomycin-resistant *E. faecium* (VRE) ATCC-2320 strain. (B) Gram-negative species: *A. baumannii* ATCC-19606, *P. aeruginosa* ATCC-9027, and *K. pneumoniae* ATCC-2146. The black bars represent the % survival of the illuminated PS-free control as a percent of the dark PS-free control, the dark blue bars represent the illuminated **Bdy$^{(2H)}$**-paper as a percent of the dark control of **Bdy$^{(2H)}$**-paper, and the light blue bars represent the illuminated **Bdy$^{(2I)}$**-paper as a percent of the dark control of **Bdy$^{(2I)}$**-paper. Illumination and assay conditions were as described in Figure 5.

PDI Studies Employing Por$^{(-)}$-Paper and Por$^{(0)}$-Paper. In vitro aPDI studies were performed to examine the effects of photosensitizer charge on paper efficacy by employing the anionic porphyrin-based **Por$^{(-)}$**-paper and the neutral porphyrin-based **Por$^{(0)}$**-paper. The materials were tested against both *S. aureus* ATCC-2913 and *A. baumannii* ATCC-19606 (Figure S1), but neither material exhibited any noteworthy photodynamic inactivation efficacy against these strains, and additional studies were not pursued due to these poor aPDI results. Given that similar porphyrin-based photosensitizers possess reasonable photophysical properties,[62] we surmise that the charge of the photosensitizer plays an important role in mediating the efficiency of PDI against bacteria in these PS-cellulose conjugates, a result that has been observed previously for solution-based photosensitizers.[63−65]

Antiviral PDI Studies Employing Por$^{(+)}$-Paper. **Por$^{(+)}$**-paper was examined for its antiviral PDI activity against three viruses (Figure 7): dengue-1, influenza A, and human adenovirus-5 (HAd-5). No inactivation of any virus was seen in the absence of paper (paper-free control) or in the presence of Whatman filter paper (PS-free paper control). However, in the presence of **Por$^{(+)}$**-paper, the dengue-1 virus was detection limit inactivated to >99.995% reduction in FFU/mL (4.5 log units; $P < 0.05$) upon illumination (30 min, 400−700 nm, 65 ± 5 mW/cm^2). When investigated against the influenza A virus, **Por$^{(+)}$**-paper was again able to achieve detection limit inactivation, although due to a difference in starting concentration, the detection limit was ~99.5% reduction in FFU/mL (2.5 log units; $P < 0.001$). Human adenovirus-5 proved the most difficult of the three viruses to inactivate, achieving ~99% reduction in FFU/mL (2 log units; $P < 0.01$). It should be noted, however, that there was more error associated with the human adenovirus-5 trials, and that the detection limit for this virus (3.5 log units) was well within one standard deviation of the average photodynamic inactivation. As was the observed for the Gram-positive bacteria, the dark controls employing **Por$^{(+)}$**-paper did initially show some inactivation of dengue-1 and influenza A when the serial

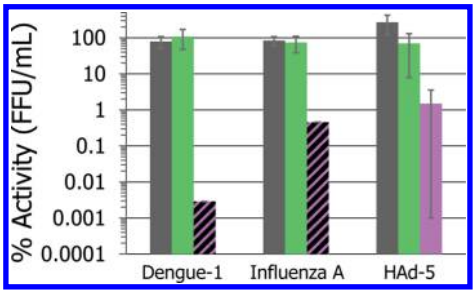

Figure 7. Antiviral photodynamic inactivation studies employing **Por$^{(+)}$**-paper against dengue-1, influenza A, and human adenovirus-5 (HAd-5). The black bars represent the % activity of the illuminated paper-free control as a percent of the dark paper-free control, the green bars represent the % activity of the illuminated PS-free control as a percent of the dark PS-free control, and the purple bars represent the illuminated **Por$^{(+)}$**-paper as a percent of the dark control of **Por$^{(+)}$**-paper. The illumination conditions and error bar visualizations were as described in Figure 5. The shaded bars represent the detection limit (see Experimental Section).

DOI: 10.1021/acs.biomac.5b00758
Biomacromolecules 2015, 16, 2482−2492

dilution step was performed under ambient room light exposure (data not shown), but this was eliminated by using low room lighting conditions (e.g., a darkroom red light that emitted at wavelengths where the photosensitizers did not absorb well).

DISCUSSION

Antimicrobial materials employing a photodynamic mechanism of action have garnered increased attention over the past decade.[66] We have previously reported on the synthesis, characterization, and efficacy of antimicrobial photodynamic inactivation of cellulose nanocrystals with a covalently attached cationic photosensitizer.[41,42] These studies demonstrated that uptake of the photosensitizer, whether into the membrane or cytoplasm, was not necessary to effectively inactivate bacteria and that photosensitizers conjugated to a cellulose solid support could have excellent antimicrobial efficacy against a diverse range of bacteria. More recently, several other studies of photosensitizers attached to solid supports, including both synthetic polymers[31,43,47,48,67,68] and a variety of cellulose-based materials,[40,44−46,69−73] have been reported. With the increased attention to aPDI functional materials, there is an increased need to better understand their pathogen scope, mechanism of action, and to increase the scientific foundation to better understand their potential to combat infectious disease.

In this work, we report the preparation of five photosensitizer-conjugated paper sheets using the Cu(I)-catalyzed Huisgen-Meldal-Sharpless 1,3-dipolar cycloaddition or "Click" reaction to conjugate alkyne-bearing photosensitizers to azide modified cellulose fibers (N_3-fibers). Demonstrating the robustness of this strategy for preparing antimicrobial photodynamic cellulose materials, a range of photosensitizers was employed, including cationic, anionic, and neutral porphyrins, as well as two neutral BODIPY-based photosensitizers, with the preparation of the PS-paper following the same chemistry previously reported for the covalent addition of a cationic porphyrin-based photosensitizer to cellulose nanocrystals.[41] Notably, only minor solvent modifications were needed to accommodate the broader range of photosensitizers and the substitution of cellulose fibers (1−4 mm in length) here versus the single photosensitizer and cellulose nanocrystals (100−400 nm) used in that previous study. The combination of thermal gravimetric analysis, gel permeation chromatography, and UV−vis diffuse reflectance spectroscopy together demonstrated that the resulting PS-paper materials were not significantly different in terms of physical or electronic structure properties when compared to the precursor fibers and photosensitizers.

FTIR spectroscopy was used to assess the loading efficiency of each photosensitizer by measuring the decrease in the azide band of the precursor N_3-fiber that is correlated to the formation of the triazole linker between the photosensitizer and the cellulose fibers. Based on the near complete absence of an azide band for $\mathbf{Bdy}^{(2H)}$-paper and $\mathbf{Por}^{(-)}$-paper, a ∼50% reduction in band area for $\mathbf{Bdy}^{(2I)}$-paper, and a ∼30% reduction for $\mathbf{Por}^{(+)}$-paper, the results suggested a loading efficiency of $\mathbf{Bdy}^{(2H)} \approx \mathbf{Por}^{(-)} > \mathbf{Bdy}^{(2I)} > \mathbf{Por}^{(+)}$. ICP-OES analysis revealed a porphyrin loading efficiency of $\mathbf{Por}^{(-)} > \mathbf{Por}^{(+)} > \mathbf{Por}^{(0)}$, with nearly the same ratio of $\mathbf{Por}^{(-)}$ to $\mathbf{Por}^{(+)}$ (3:1) observed by FTIR spectroscopy, suggesting that both measurements are in reasonable agreement for determining photosensitizer loading efficiency. As $\mathbf{Por}^{(-)}$ was conjugated to the N_3-fibers in its neutral, triprotic form, the loading efficiencies appear to suggest that neutral (or low charge density) precursor photosensitizers allow for more efficient loading. The poorer loading of $\mathbf{Por}^{(+)}$ may be attributable to electrostatic repulsion between a partially loaded $\mathbf{Por}^{(+)}$-paper and unloaded $\mathbf{Por}^{(+)}$ (**1**), thereby limiting the conjugation reaction from going to completion. At the same time, the poorer loading of $\mathbf{Por}^{(0)}$ was likely due to steric hindrance by the dodecyl alkyl chains inhibiting interaction with either the copper catalyst or with the N_3-fibers. We had originally hypothesized that sterics would be the primary determinant of photosensitizer loading efficiency, particularly between the smaller BODIPY compounds and the larger porphyrin ones, but the efficient loading of $\mathbf{Por}^{(-)}$ and the poor loading of $\mathbf{Por}^{(0)}$ suggest a more complicated interplay between charge and size, with both factors needing to be considered in the future design of photodynamic materials.

The results of the antibacterial PDI assay employing $\mathbf{Por}^{(+)}$-paper demonstrated this material to be highly effective at inactivating bacteria regardless of their taxonomic designation. Though it had the second lowest photosensitizer loading (∼30%), under the illumination conditions employed $\mathbf{Por}^{(+)}$-paper was able to eliminate ∼99.99% (∼4 log units) of each of the bacterial strains examined. The material was also found to exhibit no decrease in antimicrobial activity against *A. baumannii*, even after being preilluminated continuously for 12 h prior to the aPDI assay. This virtually identical (within error) efficacy against a range of bacteria was particularly interesting in light of our previous results with $\mathbf{Por}^{(+)}$-CNCs[41,42] that showed a significant difference in photoinactivation between the bacteria. In that previous work, greater inactivation efficiency was observed for *S. aureus* and *A. baumannii* (∼5+ log units reduction), but a lower inactivation was observed for *P. aeruginosa* (<3 log units). As to why $\mathbf{Por}^{(+)}$-CNCs showed a differential response in antibacterial PDI and $\mathbf{Por}^{(+)}$-paper did not, we suggest that the nature of the cellulose materials (paper vs nanocrystals) themselves is a major determinant. $\mathbf{Por}^{(+)}$-CNC exhibited a strong dependence (i.e., up to 2 log units more inactivation at longer times) on the incubation time of the material in the bacterial culture (prior to illumination) for effective aPDI to be achieved, whereas no such incubation time dependence was observed here with $\mathbf{Por}^{(+)}$-paper (data not shown). The incubation time dependence of $\mathbf{Por}^{(+)}$-CNC was likely due to it being suspended in the bacterial culture, and thereby led to an initially poor interaction between the photosensitizer and the bacteria. As singlet oxygen diffusion in water is limited to <250 nm,[21] the inactivation of bacteria by these materials is restricted solely to within close proximity. Thus, as the adhesion/attraction properties of the bacteria to the material surface is likely strain-dependent, the resulting photodynamic inactivation would be as well, leading to the strain-dependent photoinactivation differences observed for $\mathbf{Por}^{(+)}$-CNC. By contrast, the interaction of $\mathbf{Por}^{(+)}$-paper with bacteria was immediate as the bacterial culture was absorbed directly by the material, resulting in no strain-dependent properties governing their photodynamic inactivation being observed.

Two additional porphyrin based PS-papers were prepared, $\mathbf{Por}^{(-)}$-paper and $\mathbf{Por}^{(0)}$-paper, to explore the effects of anionic charge and increased photosensitizer hydrophobicity, respectively. Although $\mathbf{Por}^{(-)}$-paper exhibited the highest photosensitizer loading of the porphyrin-paper materials, in preliminary testing it showed less than a 1 log unit reduction in CFU/mL for *S. aureus*, and no statistically significant inactivation of *A. baumannii*. This result was not entirely unexpected given that electrostatic repulsion has been

DOI: 10.1021/acs.biomac.5b00758
Biomacromolecules 2015, 16, 2482−2492

attributed to the comparatively poor performance of anionic photosensitizers, as bacteria possess negatively charged cellular envelopes.[63] As for **Por**$^{(0)}$-paper, this material exhibited the lowest level of photosensitizer loading, and was initially so hydrophobic that the bacterial solutions beaded on its surface, preventing the interaction of the material with the bacteria. To overcome this, the material was doped with mother fibers by 50%, yet this only served to dilute the photosensitizer loading even further, and in preliminary testing, no inactivation of either *S. aureus* or *A. baumannii* was observed. While the technical limitations prevented a thorough examination of Por$^{(0)}$ (**2**) at a loading efficiency similar to that of the other photosensitizers, it may be concluded that **Por**$^{(0)}$-paper is simply too hydrophobic for this particular application.

Previous studies with water-soluble BODIPY photosensitizers found them to be highly effective for photodynamic applications in solution.[23,58,61] Given this, we prepared photosensitizer-conjugated paper sheets employing the BODIPY scaffold to determine their antimicrobial efficacy. The results of the antibacterial PDI assay employing **Bdy**$^{(2I)}$-paper demonstrated a more modest antibacterial efficacy than **Por**$^{(+)}$-paper, with the best results achieved against *A. baumannii* and *P. aeruginosa* (∼2.5 log units reduction in CFU/mL), slight inactivation of *K. pneumoniae* and *S. aureus* (∼1 log unit reduction), and no inactivation of *E. faecium*. While the **Bdy**$^{(2I)}$ (**5**) photosensitizer employed here has a lower singlet oxygen quantum yield than **Por**$^{(+)}$ (**1**),[23,41,58] a lower yield of singlet oxygen production does not explain the lower efficacy of **Bdy**$^{(2I)}$-paper when compared to **Por**$^{(+)}$-paper given the higher photosensitizer loading efficiency of the former. As such, we suggest that the simplest explanation for the reduced efficacy of **Bdy**$^{(2I)}$-paper was that the neutral and hydrophobic photosensitizer lacks the electrostatic attraction inherent in the cationic **Por**$^{(+)}$-paper that appears to be needed for efficient bacterial inactivation, with such cationic charges being a hallmark of highly efficient solution-based photosensitizers.[63−65] Interestingly, **Bdy**$^{(2I)}$-paper exhibited greater efficacy against Gram-negative strains than Gram-positive ones, and this observation may be the result of an alternative secondary interaction between the material and the bacteria that is normally unobservable due to the large (primary) electrostatic attraction that dominates with cationic photosensitizers. The origins of this observation were not further pursued, however, given the overall low inactivation observed. Finally, **Bdy**$^{(2H)}$ (**4**) was studied as a low singlet oxygen control: though structurally almost identical to **Bdy**$^{(2I)}$ (**5**), the lack of the heavy atom effect in **Bdy**$^{(2H)}$ (**4**) leads it to exhibit a large fluorescence quantum yield, which is an alternative relaxation pathway to the excitation of singlet oxygen. Demonstrating the importance of singlet oxygen production, **Bdy**$^{(2H)}$-paper showed little to no aPDI efficacy.

Given the greater efficacy of **Por**$^{(+)}$-paper against bacteria when compared to the other porphyrin- or BODIPY-based cellulose conjugates, we extended the aPDI application of this material in preliminary investigations against three viruses: dengue-1, influenza A, and human adenovirus-5. The results of the antiviral PDI assay employing **Por**$^{(+)}$-paper demonstrated detection limit inactivation of both dengue-1 virus (4.5 log units) and influenza A (2.5 log units). Human adenovirus-5 was found to be slightly more resistant to photoinactivation, but a notable 99% reduction in FFU/mL (2 log units) was still achieved. As human adenovirus-5 was the only nonenveloped virus examined, this result may suggest that the protein-based capsids of these viruses are more resistant to photosensitization than lipid-bilayer enclosed viruses. While some mechanistic studies of antiviral PDI have been reported,[30,74] further studies of nonenveloped viruses would be necessary to firmly establish this explanation. Moreover, additional studies employing neutral and anionic photosensitizers will be needed to better understand the dependence on electrostatic charge of antiviral PDI with these materials, as electrostatic effects are anticipated to be less of a factor for viruses than for bacteria. Overall, however, our preliminary study here demonstrates that materials such as **Por**$^{(+)}$-paper show exceptional promise for their application in antiviral PDI.

CONCLUSIONS

Using the Huisgen-Meldal-Sharpless 1,3-dipolar cycloaddition reaction, five photosensitizers were covalently attached to cellulose fibers and subsequently pressed into PS-paper sheets. The antibacterial efficacy of these photomicrobicidal materials was explored against taxonomically diverse bacteria, focusing on the ESKAPE pathogens *S. aureus*, *E. faecium*, *A. baumannii*, *P. aeruginosa*, and *K. pneumoniae*. Our best results were achieved with a cationic porphyrin modified paper, **Por**$^{(+)}$-paper, which was found to have broad antibacterial efficacy and unexpectedly exhibited equivalent levels of inactivation, regardless of the bacterial strain tested. These findings for **Por**$^{(+)}$-paper demonstrate a significant advance over similar cellulose nanocrystal analogs given that photoinactivation with CNC-Por was found to be strain-specific, thus, limiting potential applications. Investigations of neutral and anionic PS-papers, including BODIPY photosensitizers and two previously unreported alkyne-modified porphyrins, showed greatly reduced efficacies in comparison, suggesting that cationic charges are crucial for antibacterial efficacy, even for a materials-based aPDI approach. These results lead us to conclude that future iterations of these materials should be designed with cationic charges to be effective against bacteria, though it was not determined whether these charges must reside exclusively on the photosensitizer, and studies exploring cationic charges on the cellulose scaffold are planned. Another significant finding for cellulose-based aPDI materials was that **Por**$^{(+)}$-paper was effective against viruses, achieving detection limit inactivation of both dengue-1 virus and influenza A virus, and reasonable efficacy against human adenovirus-5. The sensitivity of **Por**$^{(+)}$-paper to ambient room light for the Gram-positive bacteria, as well as the dengue-1 and influenza A viruses, also suggests that applications may not require specialized light sources for sterilization purposes, and future antimicrobial studies will explore varying the light dose to that effect. The combined antimicrobial results obtained for **Por**$^{(+)}$-paper demonstrate the promise and potential of future iterations of scalable cellulose-based aPDI materials in hospitals and healthcare-related industries wherein novel materials that autonomously sterilize surfaces may be used to reduce the transmission of infectious disease, thereby reducing the frequency and consequences of HAIs.

ASSOCIATED CONTENT

Supporting Information

Synthesis and characterization of the precursor photosensitizers (**1**−**5**), elemental analysis of the PS-paper sheets, and photodynamic inactivation studies with Por$^{(-)}$-paper and Por$^{(0)}$-paper (Figure S1). The Supporting Information is

DOI: 10.1021/acs.biomac.5b00758
Biomacromolecules 2015, 16, 2482−2492

available free of charge on the ACS Publications website at DOI: 10.1021/acs.biomac.5b00758.

AUTHOR INFORMATION

Corresponding Author

*Tel.: +1-919-513-0680. Fax: +1-919-515-5079. E-mail: reza_ghiladi@ncsu.edu.

Notes

The authors declare no competing financial interest.

ACKNOWLEDGMENTS

This research was supported by a North Carolina State University Research Innovation and Seed Funding (RISF) Grant #2014-0793.

REFERENCES

(1) Magill, S. S.; Edwards, J. R.; Bamberg, W.; Beldavs, Z. G.; Dumyati, G.; Kainer, M. A.; Lynfield, R.; Maloney, M.; McAllister-Hollod, L.; Nadle, J.; Ray, S. M.; Thompson, D. L.; Wilson, L. E.; Fridkin, S. K. *N. Engl. J. Med.* **2014**, *370*, 1198−1208.

(2) Scott, R. D. *The Direct Medical Costs of Healthcare-Associated Infections in U.S. Hospitals and the Benefits of Prevention*; Centers for Disease Control and Prevention: Atlanta, GA, 2009; p 13.

(3) Wright, G. D. *Can. J. Microbiol.* **2014**, *60*, 147−154.

(4) Budhathoki-Uprety, J.; Peng, L.; Melander, C.; Novak, B. M. *ACS Macro Lett.* **2012**, *1*, 370−374.

(5) Jawad, A.; Snelling, A. M.; Heritage, J.; Hawkey, P. M. *J. Hosp. Infect.* **1998**, *39*, 235−240.

(6) Hirai, Y. *J. Hosp. Infect.* **1991**, *19*, 191−200.

(7) Guenthner, S. H.; Hendley, J. O.; Wenzel, R. P. *J. Clin. Microbiol.* **1987**, *25*, 488−490.

(8) Kramer, A.; Schwebke, I.; Kampf, G. *BMC Infect. Dis.* **2006**, *6*, 130.

(9) Neely, A. N.; Maley, M. P. *J. Clin. Microbiol.* **2000**, *38*, 724−726.

(10) Cimolai, N. *Eur. J. Clin. Microbiol. Infect. Dis.* **2008**, *27*, 481−493.

(11) *Self-Cleaning Materials and Surfaces: A Nanotechnology Approach*; Daoud, W. A., Ed.; John Wiley & Sons, Ltd.: Chichester, 2013.

(12) Noimark, S.; Dunnill, C. W.; Parkin, I. P. *Adv. Drug Delivery Rev.* **2013**, *65*, 570−580.

(13) Sharma, S. K.; Dai, T. H.; Hamblin, M. R. In *Antimicrobial Drug Discovery: Emerging Strategies*; Tegos, A., Mylonakis, E., Eds.; CABI: Wallingford, 2012; pp 310−322.

(14) St Denis, T. G.; Dai, T.; Izikson, L.; Astrakas, C.; Anderson, R. R.; Hamblin, M. R.; Tegos, G. P. *Virulence* **2011**, *2*, 509−520.

(15) Wainwright, M. *Int. J. Antimicrob. Agents* **2010**, *36*, 14−18.

(16) Dai, T.; Huang, Y. Y.; Hamblin, M. R. *Photodiagn. Photodyn. Ther.* **2009**, *6*, 170−188.

(17) Jori, G.; Coppellotti, O. *Anti-Infect. Agents Med. Chem.* **2007**, *6*, 119−131.

(18) Macdonald, I. J.; Dougherty, T. J. *J. Porphyrins Phthalocyanines* **2001**, *5*, 105−129.

(19) Merkel, P. B.; Kearns, D. R. *J. Am. Chem. Soc.* **1972**, *94*, 7244−7253.

(20) Bezman, S. A.; Burtis, P. A.; Izod, T. P. J.; Thayer, M. A. *Photochem. Photobiol.* **1978**, *28*, 325−329.

(21) Dahl, T. A.; Robert Midden, W.; Hartman, P. E. *Photochem. Photobiol.* **1987**, *46*, 345−352.

(22) Wainwright, M. *Int. J. Antimicrob. Agents* **2014**, *44*, 26−29.

(23) Caruso, E.; Banfi, S.; Barbieri, P.; Leva, B.; Orlandi, V. T. *J. Photochem. Photobiol., B* **2012**, *114*, 44−51.

(24) Maisch, T. *Mini-Rev. Med. Chem.* **2009**, *9*, 974−983.

(25) Muli, D. K.; Carpenter, B. L.; Mayukh, M.; Ghiladi, R. A.; McGrath, D. V. *Tetrahedron Lett.* **2015**, *56*, 3541−3545.

(26) Donnelly, R. F.; McCarron, P. A.; Tunney, M. M. *Microbiol. Res.* **2008**, *163*, 1−12.

(27) de Menezes, H. D.; Rodrigues, G. B.; Teixeira, S. d. P.; Massola, N. S., Jr.; Bachmann, L.; Wainwright, M.; Braga, G. U. *Appl. Environ. Microbiol.* **2014**, *80*, 1623−1632.

(28) Dai, T.; Fuchs, B. B.; Coleman, J. J.; Prates, R. A.; Astrakas, C.; St Denis, T. G.; Ribeiro, M. S.; Mylonakis, E.; Hamblin, M. R.; Tegos, G. P. *Front. Microbiol.* **2012**, *3*, 120.

(29) Frimannsson, D. O.; Grossi, M.; Murtagh, J.; Paradisi, F.; O'Shea, D. F. *J. Med. Chem.* **2010**, *53*, 7337−7343.

(30) Costa, L.; Faustino, M. A.; Neves, M. G.; Cunha, A.; Almeida, A. *Viruses* **2012**, *4*, 1034−1074.

(31) Lhotakova, Y.; Plistil, L.; Moravkova, A.; Kubat, P.; Lang, K.; Forstova, J.; Mosinger, J. *PLoS One* **2012**, *7*, e49226.

(32) Smetana, Z.; Mendelson, E.; Manor, J.; van Lier, J. E.; Ben-Hur, E.; Salzberg, S.; Malik, Z. *J. Photochem. Photobiol., B* **1994**, *22*, 37−43.

(33) Gaspard, S.; Tempete, C.; Werner, G. H. *J. Photochem. Photobiol., B* **1995**, *31*, 159−162.

(34) Jori, G.; Fabris, C.; Soncin, M.; Ferro, S.; Coppellotti, O.; Dei, D.; Fantetti, L.; Chiti, G.; Roncucci, G. *Lasers Surg. Med.* **2006**, *38*, 468−481.

(35) Grellier, P.; Santus, R.; Mouray, E.; Agmon, V.; Maziere, J.-C.; Rigomier, D.; Dagan, A.; Gatt, S.; Schrevel, J. *Vox Sang.* **1997**, *72*, 211−220.

(36) Tavares, A.; Carvalho, C. M.; Faustino, M. A.; Neves, M. G.; Tome, J. P.; Tome, A. C.; Cavaleiro, J. A.; Cunha, A.; Gomes, N. C.; Alves, E.; Almeida, A. *Mar. Drugs* **2010**, *8*, 91−105.

(37) Maisch, T. *Anti-Infect. Agents Med. Chem.* **2007**, *6*, 145−150.

(38) Krouit, M.; Granet, R.; Branland, P.; Verneuil, B.; Krausz, P. *Bioorg. Med. Chem. Lett.* **2006**, *16*, 1651−1655.

(39) Krouit, M.; Granet, R.; Krausz, P. *Eur. Polym. J.* **2009**, *45*, 1250−1259.

(40) Ringot, C.; Sol, V.; Granet, R.; Krausz, P. *Mater. Lett.* **2009**, *63*, 1889−1891.

(41) Feese, E.; Sadeghifar, H.; Gracz, H. S.; Argyropoulos, D. S.; Ghiladi, R. A. *Biomacromolecules* **2011**, *12*, 3528−3539.

(42) Carpenter, B. L.; Feese, E.; Sadeghifar, H.; Argyropoulos, D. S.; Ghiladi, R. A. *Photochem. Photobiol.* **2012**, *88*, 527−536.

(43) Ortiz, M. J.; Agarrabeitia, A. R.; Duran-Sampedro, G.; Bañuelos Prieto, J.; Lopez, T. A.; Massad, W. A.; Montejano, H. A.; García, N. A.; Lopez Arbeloa, I. *Tetrahedron* **2012**, *68*, 1153−1162.

(44) Mbakidi, J. P.; Herke, K.; Alves, S.; Chaleix, V.; Granet, R.; Krausz, P.; Leroy-Lhez, S.; Ouk, T. S.; Sol, V. *Carbohydr. Polym.* **2013**, *91*, 333−338.

(45) Banfi, S.; Nasini, G.; Zaza, S.; Caruso, E. *Tetrahedron* **2013**, *69*, 4845−4856.

(46) Fornili, S. L.; Sgroi, G.; Izzo, V. *J. Chem. Soc., Faraday Trans. 1* **1981**, *77*, 3049−3053.

(47) Kim, J.-O.; Lee, Y.-A.; Yun, B. H.; Han, S. W.; Kwag, S. T.; Kim, S. K. *Biophys. J.* **2004**, *86*, 1012−1017.

(48) Merchan, M.; Ouk, T. S.; Kubat, P.; Lang, K.; Coelho, C.; Verney, V.; Commereuc, S.; Leroux, F.; Sol, V.; Taviot-Gueho, C. *J. Mater. Chem. B* **2013**, *1*, 2139−2146.

(49) Klemm, D.; Philipp, B.; Heinze, T.; Heinze, U.; Wagenknecht, W. *Comprehensive Cellulose Chemistry: Fundamentals and Analytical Methods*; Wiley-VCH Verlag GmbH & Co. KGaA: Weinheim, 1998; Vol. *1*, pp 9−29.

(50) Moon, R. J.; Martini, A.; Nairn, J.; Simonsen, J.; Youngblood, J. *Chem. Soc. Rev.* **2011**, *40*, 3941−3994.

(51) Rice, L. B. *J. Infect. Dis.* **2008**, *197*, 1079−1081.

(52) Sadeghifar, H.; Filpponen, I.; Clarke, S. P.; Brougham, D. F.; Argyropoulos, D. S. *J. Mater. Sci.* **2011**, *46*, 7344−7355.

(53) TAPPI *T205 sp-02, Forming Handsheets for Physical Tests of Pulp*; TAPPI: Peachtree Corners, GA, 2002.

(54) Kačuráková, M.; Smith, A. C.; Gidley, M. J.; Wilson, R. H. *Carbohydr. Res.* **2002**, *337*, 1145−1153.

(55) Letot, L.; Lesec, J.; Quivoron, C. *J. Liq. Chromatogr.* **1980**, *3*, 1637−1655.

(56) Rubio, N.; Prat, F.; Bou, N.; Borrell, J. I.; Teixido, J.; Villanueva, A.; Juarranz, A.; Canete, M.; Stockert, J. C.; Nonell, S. *New J. Chem.* **2005**, *29*, 378−384.

DOI: 10.1021/acs.biomac.5b00758
Biomacromolecules 2015, 16, 2482−2492

(57) Feese, E. *Ph.D. Thesis*; North Carolina State University, Raleigh, NC, 2011.
(58) Carpenter, B. L.; Situ, X.; Scholle, F.; Bartelmess, J.; Weare, W. W.; Ghiladi, R. A. *Molecules* **2015**, *20*, 10604−10621.
(59) Sperandio, F. F.; Huang, Y.-Y.; Hamblin, M. R. *Recent Pat. Anti-Infect. Drug Discovery* **2013**, *8*, 108−120.
(60) Boucher, H. W.; Talbot, G. H.; Bradley, J. S.; Edwards, J. E.; Gilbert, D.; Rice, L. B.; Scheld, M.; Spellberg, B.; Bartlett, J. *Clin. Infect. Dis.* **2009**, *48*, 1−12.
(61) Banfi, S.; Caruso, E.; Zaza, S.; Mancini, M.; Gariboldi, M. B.; Monti, E. *J. Photochem. Photobiol., B* **2012**, *114*, 52−60.
(62) Lambert, C. R.; Reddi, E.; Spikes, J. D.; Rodgers, M. A.; Jori, G. *Photochem. Photobiol.* **1986**, *44*, 595−601.
(63) Feese, E.; Ghiladi, R. A. *J. Antimicrob. Chemother.* **2009**, *64*, 782−785.
(64) Wainwright, M.; Antczak, J.; Baca, M.; Loughran, C.; Meegan, K. *J. Photochem. Photobiol., B* **2014**, DOI: 10.1016/j.jphotobiol.2014.12.017.
(65) Huang, L.; Huang, Y. Y.; Mroz, P.; Tegos, G. P.; Zhiyentayev, T.; Sharma, S. K.; Lu, Z.; Balasubramanian, T.; Krayer, M.; Ruzie, C.; Yang, E.; Kee, H. L.; Kirmaier, C.; Diers, J. R.; Bocian, D. F.; Holten, D.; Lindsey, J. S.; Hamblin, M. R. *Antimicrob. Agents Chemother.* **2010**, *54*, 3834−3841.
(66) Craig, R. A.; McCoy, C. P.; Gorman, S. P.; Jones, D. S. *Expert Opin. Drug Delivery* **2015**, *12*, 85−101.
(67) Alvarez, M. G.; Gómez, M. L.; Mora, S. J.; Milanesio, M. E.; Durantini, E. N. *Bioorg. Med. Chem.* **2012**, *20*, 4032−4039.
(68) Naik, A. J. T.; Ismail, S.; Kay, C.; Wilson, M.; Parkin, I. P. *Mater. Chem. Phys.* **2011**, *129*, 446−450.
(69) Ringot, C.; Sol, V.; Barriere, M.; Saad, N.; Bressollier, P.; Granet, R.; Couleaud, P.; Frochot, C.; Krausz, P. *Biomacromolecules* **2011**, *12*, 1716−1723.
(70) Hettegger, H.; Sumerskii, I.; Sortino, S.; Potthast, A.; Rosenau, T. *ChemSusChem* **2015**, *8*, 680−687.
(71) Fernandes, S. C.; Sadocco, P.; Alonso-Varona, A.; Palomares, T.; Eceiza, A.; Silvestre, A. J.; Mondragon, I.; Freire, C. S. *ACS Appl. Mater. Interfaces* **2013**, *5*, 3290−3297.
(72) Zhuo, J.; Sun, G. *ACS Appl. Mater. Interfaces* **2013**, *5*, 10830−10835.
(73) Drogat, N.; Granet, R.; Le Morvan, C.; Begaud-Grimaud, G.; Krausz, P.; Sol, V. *Bioorg. Med. Chem. Lett.* **2012**, *22*, 3648−3652.
(74) Wong, T. W.; Huang, H. J.; Wang, Y. F.; Lee, Y. P.; Huang, C. C.; Yu, C. K. *J. Antimicrob. Chemother.* **2010**, *65*, 2176−2182.

DOI: 10.1021/acs.biomac.5b00758
Biomacromolecules 2015, 16, 2482−2492